



HAL
open science

Breakdown of the coherence effects and Fermi liquid behavior in YbAl₃ nanoparticles

E Echevarria-Bonet, D. Rojas, E Espeso, J Rodríguez Fernández, L Rodríguez Fernández, E Bauer, Sébastien Burdin, S. Magalhaes, L. Fernandez Barquín

► **To cite this version:**

E Echevarria-Bonet, D. Rojas, E Espeso, J Rodríguez Fernández, L Rodríguez Fernández, et al.. Breakdown of the coherence effects and Fermi liquid behavior in YbAl₃ nanoparticles. *Journal of Physics: Condensed Matter*, 2018, 30 (13), pp.135604. 10.1088/1361-648X/aab0c7 . hal-01815074

HAL Id: hal-01815074

<https://hal.science/hal-01815074v1>

Submitted on 13 Jun 2018

HAL is a multi-disciplinary open access archive for the deposit and dissemination of scientific research documents, whether they are published or not. The documents may come from teaching and research institutions in France or abroad, or from public or private research centers.

L'archive ouverte pluridisciplinaire **HAL**, est destinée au dépôt et à la diffusion de documents scientifiques de niveau recherche, publiés ou non, émanant des établissements d'enseignement et de recherche français ou étrangers, des laboratoires publics ou privés.



Distributed under a Creative Commons Attribution - NonCommercial - ShareAlike 4.0 International License

Breakdown of the coherence effects and Fermi liquid behavior in YbAl_3 nanoparticles

C Echevarria-Bonet^{1,3}, D P Rojas², J I Espeso³, J Rodríguez Fernández³, L Rodríguez Fernández⁴, E Bauer⁵, S Burdin⁶, S G Magalhães⁷ and L Fernández Barquín³

¹ BCMaterials, Bld. Martina Casiano, UPV/EHU Science Park, 48940 Leioa, Spain

² Dpto de Estructuras y Física de Edificación. ETSAM-Universidad Politécnica de Madrid, 28040 Madrid, Spain

³ Dpto. CITIMAC, Facultad de Ciencias, Universidad de Cantabria, 39005 Santander, Spain

⁴ SERMET, Universidad de Cantabria, 39005 Santander, Spain

⁵ Institute of Solid State Physics, TU Wien, 1040 Wien, Austria

⁶ University of Bordeaux, LOMA, UMR 5798, F-33400 Talence, France and CNRS, LOMA, UMR 5798, F-33400 Talence, France

⁷ Instituto de Física, Universidade Federal do Rio Grande do Sul, 91501-970 Porto Alegre, Brazil

E-mail: d.rojas@upm.es

Abstract

A change in the Kondo lattice behavior of bulk YbAl_3 has been observed when the alloy is shaped into nanoparticles (≈ 12 nm). Measurements of the electrical resistivity show inhibited coherence effects and deviation from the standard Fermi liquid behavior (T^2 -dependence). These results are interpreted as being due to the effect of the disruption of the periodicity of the array of Kondo ions provoked by the size reduction process. Additionally, the ensemble of randomly placed nanoparticles also triggers an extra source of electronic scattering at very low temperatures (≈ 15 K) due to quantum interference effects.

Keywords: Yb nanometric alloys, Kondo lattice, single impurity, electrical resistivity, quantum interference effects

1. Introduction

The behavior of magnetic impurities in a metallic host encapsulated by the well-known *Kondo effect* has been one of the most challenging problems in condensed matter physics [1]. This phenomenon is a fine example of development of electronic correlations in a solid, and in recent years it has witnessed a resurgence with the development of nanoelectronic devices and novel nanostructured materials [2, 3]. However, there is probably no other area where the presence of the *Kondo effect* is so fundamental as in strongly correlated electron systems (SCES) (Ce-, U-, and Yb-based compounds) [4]. Within the existing theories, the *Kondo lattice model* [5] has been successfully applied to explain the influence of the Kondo effect on the physical properties of this kind of material.

In the framework of this model, a large number of SCES can be classified as *Kondo lattice* systems, and these are viewed as a dense periodic array of magnetic ions, as opposed to single impurity systems, in which the impurities are assumed to be well separated, with no mutual coherence. The possibility that long range Fermi liquid coherence may break down in a Kondo alloy has opened new perspectives, since it may lead to the formation of non-trivial new quantum states [6–8]. Until now, this issue has mainly been experimentally explored in bulk materials by diluting the active Kondo ion with a non-magnetic one (in Ce alloys), paying a special attention to the crossover from Kondo lattice to single impurity regime detected by electrical resistivity measurements [9–13]. Less attention has been focused on Yb alloys than Ce systems, with only a few reports (see, for instance, [14–16]), where even this crossover has hardly been explored [17].

It is also remarkable that most of the reports in SCES have been constrained to macroscopically well-crystallized bulk materials. However, it appears evident that the development of molecular beam epitaxy techniques has—very recently allowed the production of two dimensional structures based on Ce Kondo lattice systems, known as ‘Kondo superlattices’ [18]. The reduction of the dimensionality results in new types of electronic state, as observed in CeIn₃-LaIn₃ superlattices, where an enhancement of the effective electron mass and non-Fermi liquid behavior were underlined [19]. Another example is the fabrication of multi-scale microstructures spanning from atomic to nanometer and mesoscopic scales in YbAl₃ alloy, showing a simultaneous enhancement of the electron and phonon transport properties [20].

Following this alternative route, novel phenomena appear when reducing the size of these materials to the nanometer scale. In particular, it is appealing to investigate more deeply the eventual variations in the relation to the role of Kondo interaction, especially in Kondo lattice compounds [21]. There are only a few examples of experimental results on Ce alloys ([22, 23] and references therein), and also some theoretical approaches (see, for instance, [24–26]). In Yb systems, a significant example is that of nanosized YbAl₃ particles, which exhibit a decrease of Yb valence with the size reduction. This decrease has been attributed to the bonding loss of the surface atoms [27]. More recently, changes in valence with size reduction in REPb₃ (RE = Eu, Yb) alloys have also been observed [28]. For nanosized YbAl₃, the bulk counterpart of this alloy is an archetypal intermediate valence system, which has been thoroughly studied in the past. The existence of energy scales related to coherence and Kondo effects allows the classification of this alloy as a Kondo lattice system [14]. Electrical resistivity results indicate a decrease in scattering around 100 K [29]. There are also broad maxima around 100 K in the magnetic susceptibility and the magnetic contribution to the specific heat related to an energy scale (Kondo temperature ($T_K = 500\text{--}670\text{ K}$)) [14, 30, 31], as also found in nanosized YbAl₃ alloys [27]. In this kind of material, with a Kondo temperature higher than 500 K, crystalline field effects are found to play a secondary role [1, 14, 30, 32]. Moreover, studies on the Yb_{1-x}Lu_xAl₃ series of alloys have shown that according to magnetic susceptibility and specific heat measurements, the appearance of a second energy scale at 40 K in the intermediate valence Kondo lattice YbAl₃ is a true coherence effect [14]. In addition, a reduction of Kondo lattice effects in Yb_{1-x}Lu_xAl₃ has been observed by soft x-ray photoelectron spectroscopy, with behavior in good agreement with the single impurity Anderson model [15]. However, it is interesting to note that details of these changes in the Kondo lattice behavior have not so far been explored by means of electrical resistivity ($\rho(T)$) measurements in this Yb-substituted series, despite its representing a valuable source of evidence to disclose the evolution of the coherence effects and the Kondo regime in strongly correlated Yb and Ce compounds. The Fermi liquid regime ($\propto T^2$) at low temperatures and coherence effects—hallmarks of Kondo lattice behavior—can easily be identified by measuring electronic transport properties.

In considering the electronic properties of nanosized YbAl₃ [27], and those of the bulk alloy noted above, it is relevant to scrutinize the influence of the size reduction on the electronic transport properties (electrical resistivity), and how the Kondo lattice behavior and the Fermi liquid ground state (T^2 dependence at low temperatures) are affected; these together constitute the main aims of this work. This will represent a definite step forward within SCES systems (Ce, Yb, U alloys). Additionally, the results are compared with that obtained for the non-magnetic reference LuAl₃ nanometric alloy, and with the effect of dilution by non-magnetic Lu in bulk YbAl₃ alloy, also using the electrical resistivity.

2. Experimental

Nanocrystalline LuAl₃ alloy was prepared by high-energy mechanical milling of a starting bulk alloy. The alloy was then crushed and milled in a planetary high-energy ball system (Retsch PM 400/2) at a rotation speed of 200 rpm, using a container and balls made of tungsten carbide—a similar procedure to that already used in the study of YbAl₃ and other Rare Earth nanoalloys [27, 33]. The bulk Yb_{0.2}Lu_{0.8}Al₃ alloy was prepared in an arc furnace from constituent elements Yb (Alfa-4N), Lu (Alfa-4N) and Al (Alfa-5N). Transmission electron microscopy (TEM) was performed in a JEOL JEM 2100 microscope. X-ray diffraction measurements were performed at room temperature with a Bruker D8 Advance diffractometer using Cu- $K\alpha$ radiation. Electronic transport properties were measured by the four probe method in a Quantum Design PPMS device. For the electrical resistivity measurements, the milled powder was first pressed in a press pellet die. A disk was then obtained, which had to be cut into a parallelepiped shape. The sample bar was of a typical length (10 mm) and area ($2 \times 2.5\text{ mm}^2$). Our in-house holder consisted of four spring-loaded pins. The pin holder was screwed on top of the sample until a certain deformation was observed in the springs. The spring-loaded pins were rounded to ensure excellent contact.

3. Results

Figure 1 shows the x-ray diffraction patterns and results of Rietveld refinement of 70h milled YbAl₃ (a) and LuAl₃ (b) alloys. The Rietveld analysis of x-ray data for 70h milled YbAl₃ alloy (Bragg factor: $R_B = 10\%$) provided the unit-cell parameter $a = 4.2037(7)\text{ \AA}$, mean grain size $D_{\text{XRD}} = 12(2)\text{ nm}$ and lattice strain $\eta = 0.37(3)\%$, in agreement with the previously reported results [27]. For the sample LuAl₃ milled for 70h, with a Bragg factor ($R_B = 7\%$), values of $a = 4.1918(4)\text{ \AA}$, $D_{\text{XRD}} = 10(2)\text{ nm}$ and $\eta = 0.64(3)\%$ are calculated. The structural characterization was completed, collecting TEM images. Figures 1(c) and (d) show representative high resolution transmission electron microscopy images of the 70h milled YbAl₃ and LuAl₃ nanoparticles. The figures show a single YbAl₃ particle with a mean diameter of 14 nm (figure 1(c)) and of 11 nm for LuAl₃

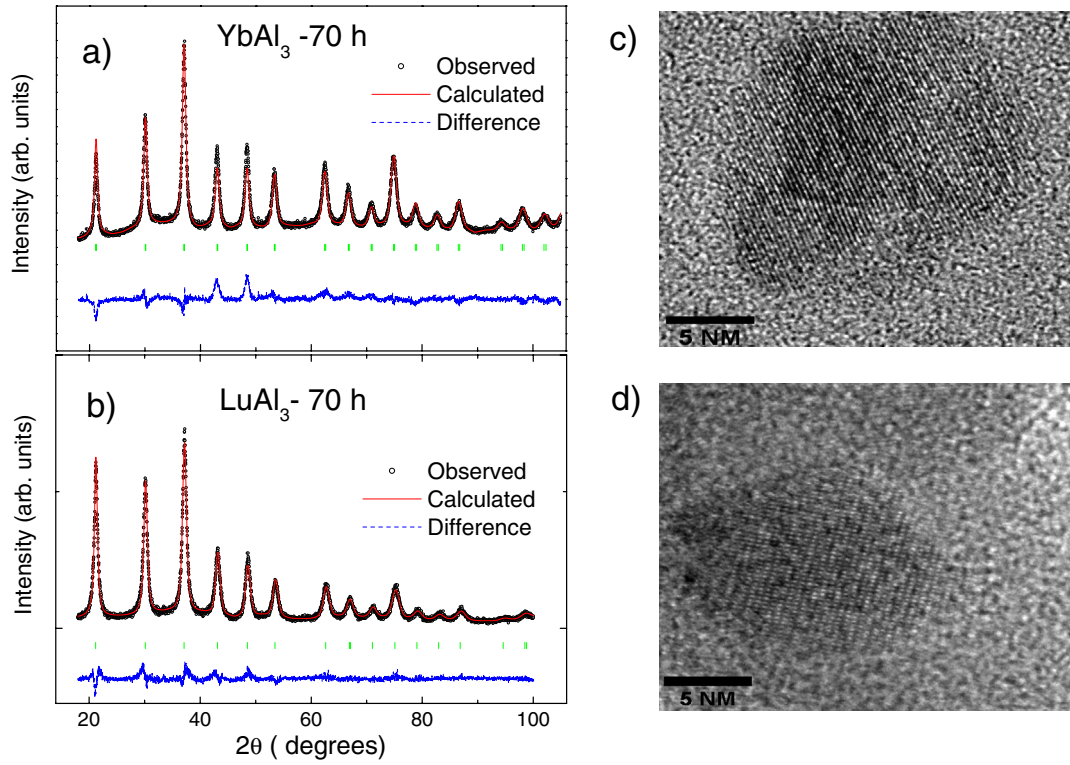


Figure 1. X-ray diffraction patterns and results of Rietveld refinement of 70h milled YbAl_3 (a) and LuAl_3 (b) alloys. The vertical markers are the expected Bragg positions according to $Pm-3m$ space group. High resolution TEM image of a nanoparticle of 70h milled YbAl_3 (c) and LuAl_3 (d) alloys.

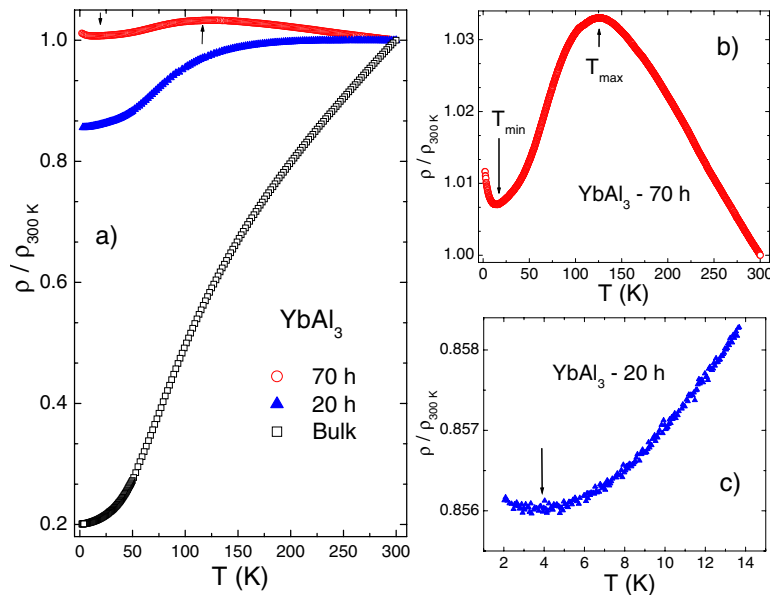


Figure 2. (a) Normalized electrical resistivity versus temperature for bulk, 20h and 70h milled YbAl_3 alloys. In the milled sample, there is a minimum followed by an increase of the resistivity, up to a broad maximum, as indicated by the markers. (b) Details of normalized electrical resistivity curve for 70h milled YbAl_3 alloy, highlighting the existence of a temperature minimum and maximum. (c) Details of the low temperature region of 20h milled YbAl_3 alloy, showing a minimum in $\rho(T)$ around 4 K.

nanoparticle (figure 1(d)). The lattice planes can be clearly observed, which indicates that the nanoparticles are crystalline at the core. These values of the mean size of the nanoparticles are near to those obtained by the analysis of the x-ray diffraction data.

Figure 2(a) shows the temperature dependence of the total electrical resistivity ($\rho(T)$) in bulk, 20h and 70h milled YbAl_3 alloys. It is observed a gradual change in the high temperature slope in the milled samples with respect to the bulk alloy, with a decrease of the relative variation in all temperature ranges

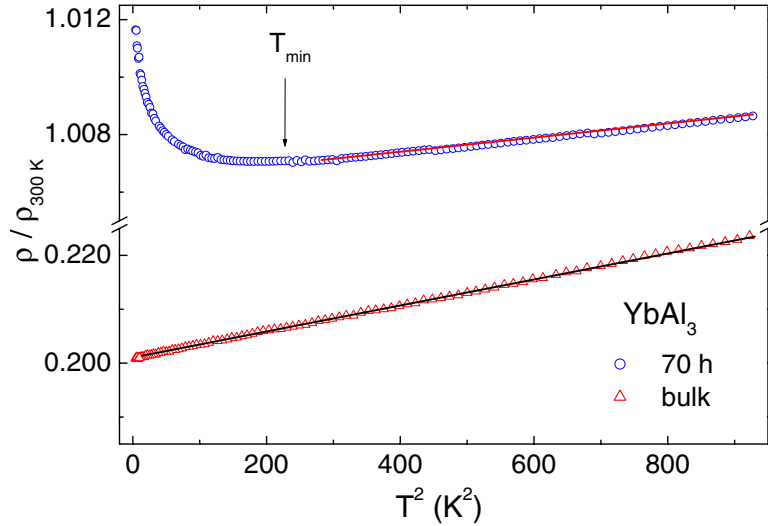


Figure 3. Details of the low temperature region of bulk and 70h milled YbAl_3 alloys, showing a deviation from the Fermi liquid dependence below T_{\min} in the nanometric alloy.

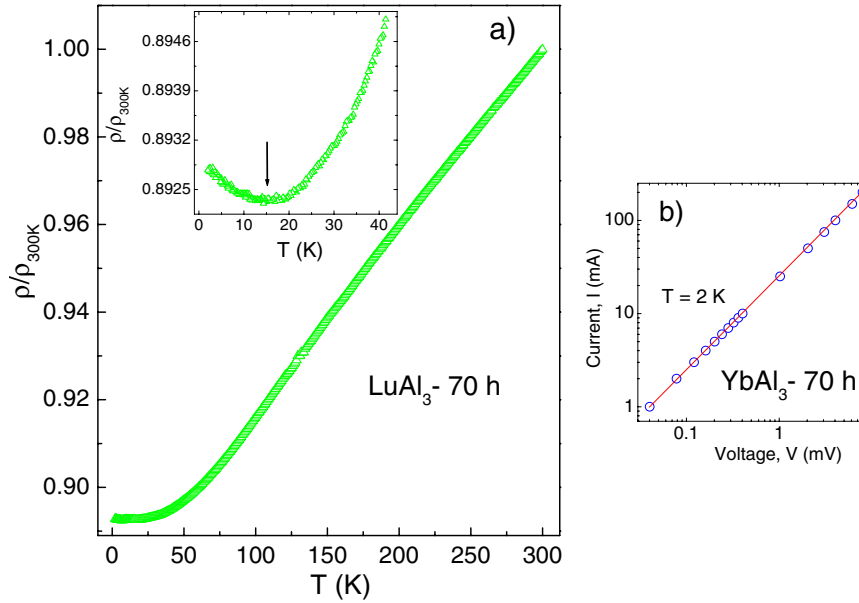


Figure 4. (a) Normalized electrical resistivity curve of the 70 milled LuAl_3 alloy. The inset details the low temperature region, showing the presence of a minimum around 15 K. (b) Curve of applied current (I) versus voltage (V) in log–log scale at 2 K in the 70h milled YbAl_3 alloy.

with the milling process. For 70h milled YbAl_3 alloy, there are two important features that indicate a remarkable difference from the bulk sample: the high temperature slope; and a minimum around 15 K, as indicated by the marker—visible in more detail in figure 2(b). There is also a broad hump in the 70h milled YbAl_3 alloy.

The appearance of this hump is typical in the magnetic contribution to $\rho(T)$ of intermediate valence Kondo lattice systems—as observed, for instance, in intermediate-valence YbCuAl [34]. When coming down from high temperatures in 70h milled YbAl_3 , the $\rho(T)$ increase can be attributed to the incoherent Kondo scattering (high temperature scale- $T_K = 670$ K [14]) until the decrease below $T_{\max} = 125$ K. Thus, the contribution to the electrical resistivity in 70h milled

YbAl_3 (see figure 2(b)) basically comes from the magnetic scattering and the residual resistivity terms. This suggests that the disorder provoked by the milling process induces an increase of scattering by defects in the crystal lattice, starting to play a more significant role than electron–phonon scattering. This fact has been observed in other milled Rare Earth-based alloys, where the electrical resistivity has shown a significant reduction of the high temperature slope with the increase of the milling time, with values of residual resistivity ratio ($\text{RRR} = \rho_{300\text{K}}/\rho_{4\text{K}}$) changing from 1.6 to 1.1 [35].

On the other hand, a drastic change (although relatively reduced) in the behavior is observed at low temperatures in such a milled sample with respect to the bulk alloy, with a marked upturn and the presence of a minimum around 15 K,

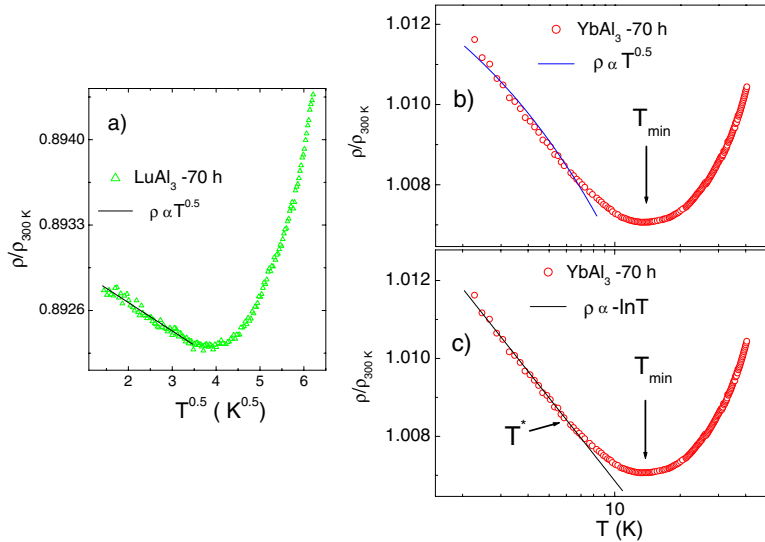


Figure 5. (a) Low temperature region of electrical resistivity described by a $-\sqrt{T}$ term in 70 h milled LuAl_3 . Fitting of the electrical resistivity data in 70 h milled YbAl_3 alloy in logarithmic scale, according to $-\sqrt{T}$ term (b) and a $-\ln T$ dependence (c). In the Yb alloy, the data is better described by $-\ln T$ behavior below $T^* = 7$ K.

as shown in figures 2(a) and (b). Specifically, there is a small upturn in YbAl_3 20 h ($\langle D_{\text{XRD}} \rangle \approx 19$ nm [27]), which demonstrates that the appearance of the minimum at 70 h alloy is not casual but the result of a definite tendency (see figure 2(c)). The consequence of this minimum is a deviation from standard Fermi liquid behavior, as shown in figure 3, when comparing the bulk and 70 h milled YbAl_3 alloy samples.

To analyze the origin of such a minimum in $\rho(T)$, it is pertinent to check $\rho(T)$ in LuAl_3 milled for 70 h. This will make it possible to test whether the minimum is observed in a conventional metallic alloy of a similar nanometric structure. In this case (see figure 4(a)), the shape of the resistivity curve is that of a typical metal. Curiously, it also displays a minimum—much shallower than that in 70 h milled YbAl_3 —as shown in detail in the inset of figure 4(a). This last feature could be intuitively interpreted as being due to additional contributions around the minimum in the Yb-based alloy, which conjecture we will address below.

The analysis of the different contributions to $\rho(T)$ in disordered (amorphous) metals and nanocrystalline alloys is not a simple task. Several mechanisms exist that could provide a reasonable interpretation for the increase of the electrical resistivity at low temperatures for the nanometric 70 h milled YbAl_3 and LuAl_3 alloys. To facilitate the interpretation, we will describe our rationale step-by-step. Firstly, it could be expected the low temperature upturn be due to eventual changes in the density of carriers, which are commonly found in semiconducting materials and hopping conductivity. In the second step, we will discuss quantum interference effects (QIE) usually observed in compounds of amorphous nature [36, 37]. Finally, a third plausible approach to quantify is the role of an eventual Kondo effect in the Yb sample; this will be discussed as another extra scattering source frequently present in SCES Yb alloys.

Regarding the first mechanism, our $\rho(T)$ measurements indicated an ohmic dependence (see figure 4(b)), thus

providing *reasonable evidence for metallic conductivity*. This rules out the influence of oxides such as Yb_2O_3 on $\rho(T)$. The presence of this oxide (less than 3% of the sample) has been previously detected in bulk and milled YbAl_3 alloys [27]. Consequently, this ohmic dependence of $\rho(T)$ also eliminates the possibility of hopping conductivity, based on Mott metal-insulator transition, at least with an exponential dependence [38]. Secondly, an electrical resistivity minimum has been widely observed in amorphous materials of high ρ_0 ($\gtrsim 80 \mu\Omega$ cm). The high-energy milling process usually leads to sizeable lattice strains and deformations, thus giving rise to a poorly crystallized environment at the very local scale [39]. Therefore, it would not be surprising to detect some influence of these effects on $\rho(T)$. Quantum electron interaction effects [36] entail two corrections, namely the electron-electron interaction (EEI) and the weak localization (WL). In the following, we will briefly comment on both effects. Although EEI and WL introduce temperature dependent corrections to resistivity, in three-dimensional disordered metals at low temperatures, the contribution to resistivity from the EEI effects dominates over that due to WL effects [36, 40]. Assuming the existence of EEI, the correction to conductivity (σ) is derived as

$$\Delta\sigma_{ee} = \frac{1.3}{\sqrt{2}} \frac{e^2}{2\pi h} F_0 \sqrt{\frac{2\pi k_B T}{hD'}}, \quad (1)$$

where $D' = \frac{v_F^2 \tau}{3}$ is the diffusion constant, in terms of the Fermi velocity v_F and the relaxation time τ . F_0 is a screening term which equals 4/3 in the absence of any applied magnetic field. Experimental reports revealing the $\rho \propto -\sqrt{T}$ dependence have been extensively published for disordered metals [37]. On the other hand, electron wave propagation—away from a classical interpretation—allows a variety of paths, with the existence of loops of interference between the electron waves, giving rise to an effective localization. If all particles returned

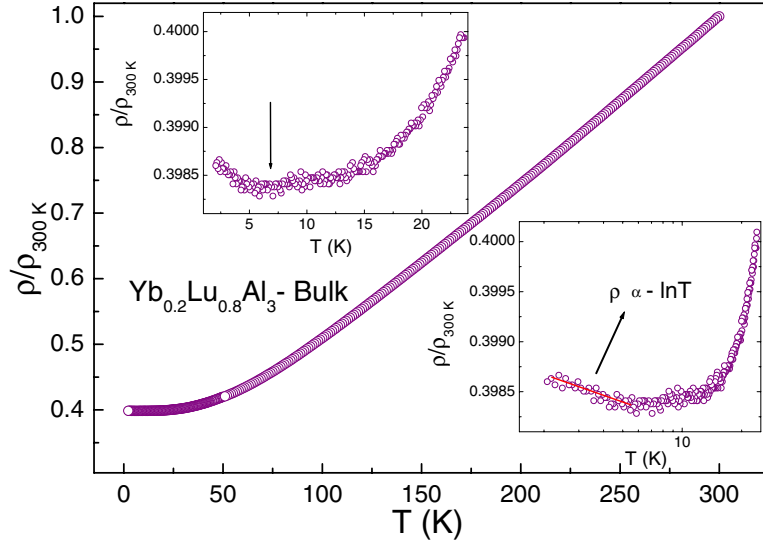


Figure 6. Normalized electrical resistivity curve of $\text{Yb}_{0.2}\text{Lu}_{0.8}\text{Al}_3$ bulk alloy. Details of the low temperature region showing the presence of a minimum around 7 K (left inset), with an upturn according to $-\ln T$ dependence (right inset).

back to the origin, then $\rho \rightarrow \infty$, and full localization would be achieved.

An ideal approach to determine the influence of EEI effects is thus to include $\rho \propto -\sqrt{T}$. As shown in figure 5(a), it is possible to fit a linear variation (\sqrt{T} dependence) for 70h milled LuAl_3 alloy. This supports, experimentally, the former assumption: the mechanism related to the electrical resistivity minimum in LuAl_3 is that due to quantum corrections.

Regarding the YbAl_3 nano (70h milled alloy), the contribution below the minimum shows an extra contribution. Let us first consider that for $T < T_{\min}$ there is a major contribution from QIE effects, as occurs in LuAl_3 . The fit considering only the $-\sqrt{T}$ term is not satisfactory (see figure 5(b)), thus suggesting the presence of (an)other, more important, scattering mechanism(s). In the SCES Yb systems we presented above, there could exist a contribution stemming from the Kondo effect ($\rho \propto -\ln(T)$) [1]. In this sense, we have found that the low temperature data ($T < 7\text{ K}$), is well described according to the $-\ln T$ dependence; the results are displayed in figure 5(c). This could indicate the presence of an additional temperature scale ($T^* = 7\text{ K}$) related to the onset of an eventual Kondo contribution at low temperatures, different from the high T_K temperature scale.

4. Discussion

The outcome of the foregoing analysis is that the experimental evidence is explained by both QIE and Kondo interaction, which are responsible for the low temperature upturn below T_{\min} . The milling of the bulk YbAl_3 results in an ensemble of nanoparticles randomly dispersed and in contact, forming a granular alloy. It is commonly accepted that nanoparticles can be generally described as a two-component system, consisting of core nanocrystallites and grain or interphase boundary components [41]. The thickness of the grain boundary is commonly assumed around 1 nm. At grain boundaries, more disorder is expected, as compared to the core of nanoparticles.

On the one hand, the nanometric size of the particles favors the presence of surface shells in which the atomic coordination is reduced whereas the microstrain is enhanced. In this situation the nanostructure becomes more and more disordered, affecting the electrical resistivity. Therefore, such considerable disorder is the basic element supporting the QIE.

In bulk YbAl_3 , the f -electron atoms form periodic arrays which lie in the so-called Kondo lattice systems [5]. Every spin in the lattice is screened by the conduction electrons. In real space, the screening takes place on a length scale of mesoscopic size ($\xi_K = \hbar v_F / k_B T_K$, where v_F is the Fermi velocity), denoted as the Kondo screening cloud [42]. The values of Fermi velocity may range from 10^6 m s^{-1} for normal metals to $10^3\text{--}10^4\text{ m s}^{-1}$ in heavy fermion systems [43]. Consequently, the Fermi velocity is directly proportional to the electronic contribution to the specific heat (Sommerfeld coefficient (γ)). The value of $\gamma = 45\text{ mJ mol}^{-1}\text{ K}^{-2}$ estimated from the specific heat data in bulk YbAl_3 is found to decrease down to $36\text{ mJ mol}^{-1}\text{ K}^{-2}$ for the 70h milled YbAl_3 alloy [27]. Since a Fermi velocity value $v_F = 4 \cdot 10^4\text{ m s}^{-1}$ is observed for bulk YbAl_3 [44], a simple scaling with the variation of the coefficient γ leads to an appraisal of $5 \cdot 10^4\text{ m s}^{-1}$ for the Fermi velocity in the milled sample. On the other hand, from the maximum in the magnetic susceptibility and magnetic contribution to the specific heat in bulk and milled YbAl_3 alloys [27], the T_K values do not change significantly, being around 500 K–670 K, as estimated for the bulk sample [14, 30, 32]. Thus, following the above reasoning, it is possible to estimate a value of ξ_K around 0.7 nm for the 70h milled YbAl_3 alloy. The length scale ξ_K would be less than the mean size of our samples (12 nm), and consequently the Kondo screening cloud is restricted within nanoparticles, at least in the core, with variations at the nanoparticle surface. The size effect would not be essential for the disruption of the Kondo lattice behavior, as the characteristic length is one order of magnitude lower than the mean grain size, whereas the increase in lattice strain and disorder at the surface of the particles with the size reduction

process will play a significant role. Our measurements of electrical resistivity of nanosized YbAl₃ indicate that the nanoparticle ensemble provokes breakdown of the Kondo lattice coherence, with an upturn at low temperatures.

It has been shown that the reduction of particle size in nano-YbAl₃ results in Yb valence reduction as a consequence of increasing numbers of non-magnetic Yb²⁺ atoms at the surface of nanoparticles [27]. Irrespective of this qualitative interpretation, what is clear is that by reducing the size, a $\rho(T)$ minimum appears with the low temperature upturn. As a matter of fact, this situation resembles the cases of bulk alloys under chemical substitution, in which by adding non-magnetic rare-earth atoms (Y and La for Ce-based and La or Lu for Yb-based compounds) a transition from Kondo lattice to single impurity regime is observed (see for instance [12, 17]. In bulk YbAl₃ the coherence scattering is maintained throughout the alloy as a result of Kondo lattice behavior. This is greatly modified whenever there is a reduction of size and a concomitant increase of surface strain and disorder in the nanoparticle shell. For comparison purposes, the possibility of a change of regime on dilution with Lu was explored in the bulk YbAl₃. The bulk sample Yb_{0.2}Lu_{0.8}Al₃ is found to crystallize in the same type of structure and space group *Pm-3m* as YbAl₃ and LuAl₃ alloys but with a lattice parameter $a = 4.1932(2)$ Å. The results show the presence of a low temperature minimum in $\rho(T)$ of the bulk Yb_{0.2}Lu_{0.8}Al₃ alloy, with an upturn following a $-\ln T$ dependence (see figure 6). Curiously, the position of this minimum, around 7 K, coincides with the onset of $-\ln T$ term below the temperature scale T^* , associated with the low temperature upturn in the 70h milled YbAl₃ alloy. Consequently, it is possible to find some similarities between the processes of size reduction and chemical substitution by Lu in bulk YbAl₃ alloy. In both cases, there is an increase in the fraction of non-magnetic atoms (Yb²⁺ or Lu) and the disorder, leading to a limit situation where the periodicity of the Kondo ions is broken. Consequently, a deviation from the Fermi liquid regime is observed.

Concerning the observed $-\ln T$ dependence of the low temperature upturn in the 70h milled YbAl₃ alloy, it is obvious that the electronic transport in an ensemble of nanoparticles is complex. It will require further study in order to ascribe it to Kondo behavior.

5. Conclusions

It is concluded that the size—in intimate combination with the increasing strain—is a significant driving parameter for intrinsic electronic scattering changes. In this context—extending the universality of the former assertion—it is widely known that particles of noble metals in nanocrystalline state can undergo serious changes in the density of states, as has been reported recently [45]. Thus, our finding is naturally connected with a more general physical situation.

To summarize, the scrutiny of the electrical resistivity in nano-YbAl₃ particles has revealed a deviation from the Fermi liquid behavior at low temperatures. This deviation is due to the combined effect of the disruption of the periodicity of the

Kondo ions (as a consequence of the size reduction process) and QIE (favored by the presence of a disordered collection of nanoparticles).

Acknowledgments

This work was supported by the Spanish MINECO under project MAT2014-55049-C2-R.

ORCID iDs

C Echevarria-Bonet  <https://orcid.org/0000-0002-3959-9124>

D P Rojas  <https://orcid.org/0000-0002-5620-8586>

J I Espeso  <https://orcid.org/0000-0002-4018-7186>

E Bauer  <https://orcid.org/0000-0001-7376-5897>

S Burdin  <https://orcid.org/0000-0003-3710-9563>

L Fernández Barquín  <https://orcid.org/0000-0003-4722-3722>

References

- [1] Hewson A C 1997 *The Kondo Problem to Heavy Fermions* (Cambridge: Cambridge University Press)
- [2] Goldhaber-Gordon D, Shtrikman H, Mahalu D, Abusch-Magder D, Meirav U and Kastner M A 1998 *Nature* **391** 156
- [3] Prüser H, Dargel P E, Bouhassoune M, Ulbrich R G, Pruschke T, Lounis S and Wenderoth M 2014 *Nat. Commun.* **5** 5417
- [4] Coleman P 2007 *Handbook of Magnetism and Advanced Magnetic Materials* ed H Kronmüller and S Parkin (Chichester: Wiley)
- [5] Doniach S 1977 *Physica B+C* **91** 231
- [6] Burdin S and Fulde P 2007 *Phys. Rev. B* **76** 104425
- [7] Kaul R K and Vojta M 2007 *Phys. Rev. B* **75** 132407
- [8] Burdin S and Lacroix C 2013 *Phys. Rev. Lett.* **110** 226403
- [9] Lawrence J M, Graf T, Hundley M F, Mandrus D, Thompson J D, Lacerda A, Torikachvili M S, Sarrao J L and Fisk Z 1996 *Phys. Rev. B* **53** 12559
- [10] Bud'ko S L, Fontes M B and Baggio-Saitovitch E M 1998 *J. Phys.: Condens. Matter* **10** 8815
- [11] Chudinov S, Brando M, Marcelli A and Battisti M 1998 *Physica B* **244** 154
- [12] Medina A N, Rojas D P, Gandra F G, Azanha W R and Cardoso L P 1999 *Phys. Rev. B* **59** 8738
- [13] Pikul A P, Stockert U, Steppke A, Cichorek T, Hartmann S, Caroca-Canales N, Oeschler N, Brando M, Geibel C and Steglich F 2012 *Phys. Rev. Lett.* **108** 066405
- [14] Bauer E D, Booth C H, Laurence J M, Hundley M F, Sarrao J L, Thompson J D, Riseborough P S and Ebihara T 2004 *Phys. Rev. B* **69** 125102
- [15] Yamaguchi J, Sekiyama A, Imada S, Yamasaki A, Tsunekawa M, Muro T, Ebihara T, Onuki Y and Suga S 2007 *New J. Phys.* **9** 317
- [16] Köhler U, Oeschler N, Steglich F, Maquilon S and Fisk Z 2008 *Phys. Rev. B* **77** 104412
- [17] Rojas D P, Medina A N, Gandra F G, Fernández Barquín L and Gómez Sal J C *Physica B* accepted (<https://doi.org/10.1016/j.physb.2017.09.096>)
- [18] Shimozawa M, Goh S K, Shibauchi T and Matsuda Y 2016 *Rep. Prog. Phys.* **79** 074503
- [19] Shishido H, Shibauchi T, Yasu K, Kato T, Kontani H, Terashima T and Matsuda Y 2010 *Science* **327** 980
- [20] He D *et al* 2017 *J. Alloys Compd.* **725** 1297–303

- [21] Lonzarich G, Pines D and feng Yang Y 2017 *Rep. Prog. Phys.* **80** 024501
- [22] Chen Y Y, Huang P H, Ou M N, Wang C R, Yao Y D, Lee T K, Yao M Y, Laurence J M and Booth C H 2007 *Phys. Rev. Lett.* **98** 157206
- [23] Mohanta S K, Mishra S N, Iyer K K and Sampathkumaran E V 2013 *Phys. Rev. B* **87** 125125
- [24] Thimm W B, Kroha J and von Delft J 1999 *Phys. Rev. Lett.* **82** 2143
- [25] Hand T, Kroha J and Monien H 2006 *Phys. Rev. Lett.* **97** 136604
- [26] Schwabe A, Gütersloh D and Potthoff M 2012 *Phys. Rev. Lett.* **109** 257202
- [27] Rojas D P, Barquín L F, Espeso J I and Rodríguez Fernández J 2008 *Phys. Rev. B* **78** 094412
- [28] Subbarao U, Sarkar S, Jana R, Bera S S and Peter S C 2016 *Inorg. Chem.* **55** 5603–11
- [29] Rowe D M, Kuznetsov V L, Kuznetsova L A and Min G 2002 *J. Phys. D: Appl. Phys.* **35** 2183
- [30] Cornelius A L *et al* 2002 *Phys. Rev. Lett.* **88** 117201
- [31] Burdin S, Georges A and Grempel D R 2000 *Phys. Rev. Lett.* **85** 1048
- [32] Ebihara T, Bauer E D, Cornelius A L, Laurence J M, Harrison N, Thompson J D, Sarrao J L, Hundley M F and Uji S 2003 *Phys. Rev. Lett.* **90** 166404
- [33] Rojas D P, Barquín F, Fernández J R, Espeso J I and Sal J C G 2007 *J. Phys.: Condens. Matter* **19** 186214
- [34] Schlottmann P 1989 *Phys. Rep.* **181** 1
- [35] Echevarria-Bonet C *et al* 2015 *J. Phys.: Condens. Matter* **27** 496002
- [36] Lee P A and Ramakrishnan T V 1985 *Rev. Mod. Phys.* **57** 287
- [37] Howson M A and Gallagher B L 1988 *Phys. Rep.* **170** 265
- [38] Kittel C 1986 *Introduction to Solid State Physics* (New York: Wiley)
- [39] Echevarria-Bonet C *et al* 2013 *Phys. Rev. B* **87** 180407
- [40] Ghosh T, Fukuda T, Kakeshita T, Kaul S N and Mukhopadhyay P K 2017 *Phys. Rev. B* **95** 140401
- [41] Rojas D P, Barquín L F, Fernández J R, Fernández L R and Gonzalez J 2010 *Nanotechnology* **21** 445702
- [42] Park J, Lee S S B, Oreg Y and Sim H S 2013 *Phys. Rev. Lett.* **110** 246603
- [43] Mourachkine A 2004 *Room-Temperature Superconductivity* (Cambridge: Cambridge International Science Pub.)
- [44] Demsar J, Kabanov V V, Alexandrov A S, Lee H J, Bauer E D, Sarrao J L and Taylor A J 2009 *Phys. Rev. B* **80** 085121
- [45] Garitaonandia J S *et al* 2008 *Nano Lett.* **8** 661